

Critical thickness for the two-dimensional electron gas in $\text{LaTiO}_3/\text{SrTiO}_3$ superlatticesJeong Ho You^{1,*} and Jun Hee Lee²¹*Department of Mechanical Engineering, Southern Methodist University, Dallas, Texas, USA*²*Department of Chemistry, Princeton University, Princeton, New Jersey, USA*

(Received 30 May 2013; revised manuscript received 16 September 2013; published 8 October 2013)

Transport dimensionality of Ti d electrons in $(\text{LaTiO}_3)_1/(\text{SrTiO}_3)_N$ superlattices has been investigated using density functional theory with local spin-density approximation + U method. Different spatial distribution patterns have been found between Ti t_{2g} orbital electrons. The d_{xy} orbital electrons are highly localized near interfaces due to the potentials by positively charged LaO layers, while the degenerate d_{yz} and d_{xz} orbital electrons are more distributed inside SrTiO_3 insulators. For $N \geq 3$ unit cells (u.c.), the Ti d_{xy} densities of state exhibit the staircaselike increments, which appear at the same energy levels as the d_{xy} flat bands along the Γ -Z direction in band structures. The k_z -independent discrete energy levels indicate that the electrons in d_{xy} flat bands are two-dimensional electron gases (2DEGs) which can transport along interfaces, but they cannot transport perpendicularly to interfaces due to the confinements in the potential wells by LaO layers. Unlike the d_{xy} orbital electrons, the d_{yz} and d_{xz} orbital electrons have three-dimensional (3D) transport characteristics, regardless of SrTiO_3 thicknesses. The 2DEG formation by d_{xy} orbital electrons, when $N \geq 3$ u.c., indicates the existence of critical SrTiO_3 thickness where the electron transport dimensionality starts to change from 3D to 2D in $(\text{LaTiO}_3)_1/(\text{SrTiO}_3)_N$ superlattices.

DOI: [10.1103/PhysRevB.88.155111](https://doi.org/10.1103/PhysRevB.88.155111)

PACS number(s): 73.20.-r, 73.21.-b

I. INTRODUCTION

Recent discoveries of thin metallic layers in heterostructures composed of perovskite oxide insulators have motivated many research activities to understand the origin and properties of conducting carriers.^{1–4} In these heterostructures, electrons are strongly localized near interfaces to form two-dimensional electron gases (2DEGs).^{5,6} Since 2DEGs have been successfully utilized in semiconductor transport and optical devices,^{7,8} perovskite oxide heterostructures with 2DEGs are of great interest to advance oxide electronics with novel functionalities.⁴ Especially, SrTiO_3 -based structures [e.g., $\text{LaAlO}_3/\text{SrTiO}_3$ (LAO/STO) (Refs. 6 and 9), $\text{LaTiO}_3/\text{SrTiO}_3$ (LTO/STO) (Refs. 10 and 11), $\text{SrTiNbO}_3/\text{SrTiO}_3$ (STNO/STO) (Refs. 12–15), etc.] have been intensively investigated and exhibited many intriguing physical properties including high mobility,^{5,16,17} superconductivity,^{15,18,19} electric-field controlled resistance,²⁰ novel magnetism,^{21–23} and large thermoelectric power.^{12–14,24}

In LAO/STO heterostructures, where both constituents are wide band gap insulators, there exists the critical LAO film thickness of 4 unit cells (u.c.) to become conducting.²⁵ However, LTO/STO heterostructures exhibit a metallic behavior even with a single u.c. of LTO (Refs. 5 and 17). An LTO is a Mott insulator with an occupied Ti $3d^1$ state, while a STO is a band gap insulator with an empty Ti $3d^0$ state. When a LTO is adjoined to a STO, Ti cations in TiO_2 layers between adjacent LaO and SrO layers begin to have an averaged valence of $3d^{0.5}$ (Refs. 26 and 27). This electronic reconstruction induces the metallic LTO/STO interfaces with the carrier density of $\sim 0.5e/\text{u.c.}$ per interface.⁵ Ohtomo *et al.*¹ have found the leakage of Ti $3d$ electrons from the interfacial TiO_2 layers into a few unit cells of STO. Density functional theory (DFT) calculations have revealed that the extent of Ti $3d$ electrons strongly depends on the screening of potentials induced by positively charged LaO layers.^{28–30} Tunability of transport properties has been investigated by fractional doping such as $\text{La}_x\text{Sr}_{1-x}\text{TiO}_3/\text{SrTiO}_3$ and $\text{SrTi}_y\text{Nb}_{1-y}\text{O}_3/\text{SrTiO}_3$ structures.^{11–13,31}

In this study, we investigate the effects of STO spacers on transport dimensionality in $(\text{LTO})_1/(\text{STO})_N$ superlattices grown on STO substrate. Since both LTO and STO have a common TiO_2 layer, the $(\text{LTO})_1/(\text{STO})_N$ superlattices have a LaO layer replacing a SrO layer in every $(N + 1)$ u.c. along the $[001]$ growth direction. With varying the STO spacer thickness, we are controlling the separation distance between the LaO-induced potential wells to examine the changes of electron transport properties.

II. CALCULATION DETAILS

DFT calculations have been used to investigate the $(\text{LTO})_1/(\text{STO})_N$ superlattices with various STO thicknesses as $N = 1$ –10 u.c. All calculations were performed using the Vienna *Ab initio* Simulation Package (VASP)^{32,33} with the projector-augmented wave approach,³⁴ the energy cutoff of 500 eV, and the rotationally invariant local spin-density approximation (LSDA) + U method.³⁵ We used $U = 5$ eV and $J = 0.64$ eV for Ti d states,^{30,36} and $U_f = 11$ eV and $J_f = 0.68$ eV for La f states.³⁰ The in-plane (xy plane) lattice constants were fixed as the experimental value of 3.91 Å for cubic STO to simulate the boundary condition by the STO substrate.¹ The out-of-plane (z direction) lattice vector was optimized within the tetragonal $P4mm$ space group, and all ionic positions were relaxed until all Hellmann-Feynman forces were smaller than 5 meV/Å. After self-consistent calculations were performed with a $6 \times 6 \times n$ k -point grid where $n \approx 6/(N + 1)$ to optimize the lattice vector and ionic positions, non self-consistent calculations were carried out with a finer k -point grid of $24 \times 24 \times n$ where $n \approx 24/(N + 1)$.

III. RESULTS AND DISCUSSION

The calculated relaxed structure for the $(\text{LTO})_1/(\text{STO})_8$ superlattice is shown in Fig. 1(a) as an example. In the relaxed structure, the negatively charged O atoms move toward the

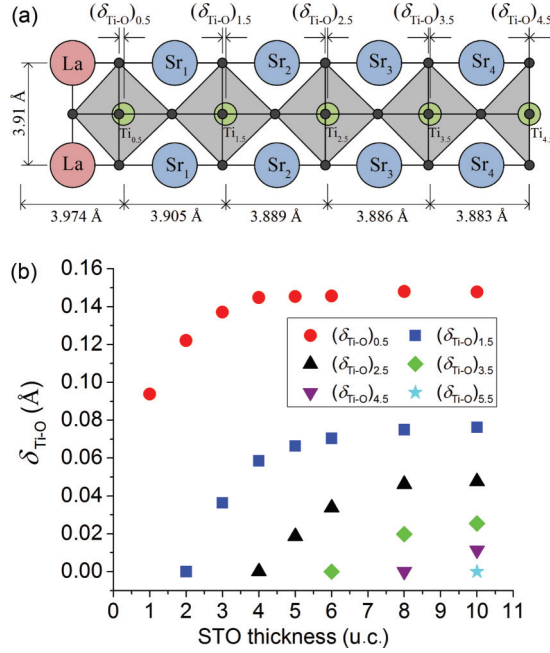


FIG. 1. (Color online) (a) Calculated relaxed structure for the $(\text{LTO})_1/(\text{STO})_8$ superlattice as an example. (b) Relative Ti-O displacements ($\delta_{\text{Ti-O}}$) as a function of STO thickness in $(\text{LTO})_1/(\text{STO})_N$ superlattices.

positively charged LaO layer due to Coulomb force. This ferroelectriclike TiO₆ octahedra distortion is known to provide ionic screening in addition to electronic screening to the potentials by LaO layers, and, as a result, the Ti *d* electrons are spread widely over a few unit cells of STO.^{28–30} The relative Ti-O displacements ($\delta_{\text{Ti-O}}$) are shown in Fig. 1(b) as a function of STO thickness. The largest $\delta_{\text{Ti-O}}$ always occurs at the interfacial TiO₂ layer (Ti_{0.5}), and the magnitude of $\delta_{\text{Ti-O}}$ decays rapidly as moving away from the interface. As the STO thickness increases, the magnitude of $\delta_{\text{Ti-O}}$ increases and gets converged. For $N = 3-4$ u.c., the magnitude of $(\delta_{\text{Ti-O}})_{0.5}$ is converged to ~ 0.14 Å.

Spatial distributions of Ti *d* electrons have been calculated for different STO spacer thicknesses, as shown in Fig. 2. The *d* electron charges are obtained by integrating the occupied states in Ti 3*d* densities of states (DOS; shown in Fig. 3) and normalized to have 0.5*e*/u.c. per interface [i.e., 1*e*/u.c. per LTO cell in $(\text{LTO})_1/(\text{STO})_N$ superlattices]. The positively charged LaO layers are located at the periodic positions of $0, \pm(N+1), \pm 2(N+1), \dots$. Different distribution patterns can be observed between Ti *t*_{2g} orbitals. The *d*_{xy} orbital electrons are highly localized near the interfaces, and its occupancy decays fast inside the STO insulators. With increasing the STO spacer thickness, the neighboring *d*_{xy} electrons become almost separated. As an example, in the $(\text{LTO})_1/(\text{STO})_{10}$ superlattice, the *d*_{xy} electron charges are only 0.0055*e* and 0.0051*e* at the Ti_{4.5} and Ti_{5.5} sites, respectively. The high occupancy at the interfaces indicates that the *d*_{xy} orbital is strongly influenced by the LaO-induced potential wells. In contrast to the *d*_{xy} orbital, the degenerate *d*_{yz} and *d*_{xz} orbitals are more occupied inside the STO insulators. Also, the occupancy of *d*_{yz} (*d*_{xz}) orbital decreases drastically and becomes almost homogeneous with the increase of STO thickness.

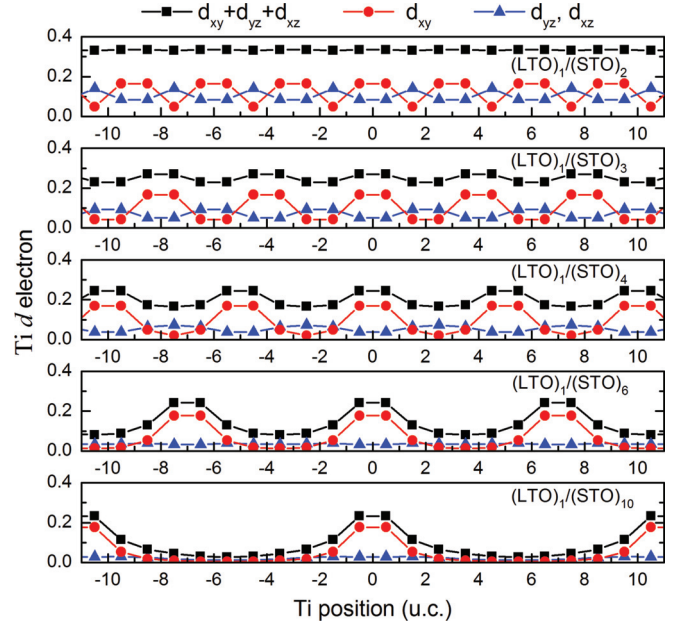


FIG. 2. (Color online) Spatial distributions of Ti 3*d* electrons in $(\text{LTO})_1/(\text{STO})_N$ superlattices. Ti *d* electron densities are normalized to have 0.5*e*/u.c. per interface. The positively charged LaO layers are located at the periodic positions of $0, \pm(N+1), \pm 2(N+1), \dots$.

Figure 3 shows the calculated Ti 3*d* DOS for conduction bands with various STO spacer thicknesses. The Fermi level is at 0 eV. At each Ti site, the DOS with spin-up (spin-down) states is shown in the upper (lower) panel. From the integration of DOS between midgap and the Fermi level, the *d* electron density of $\sim 0.7e$ /u.c. has been obtained. In the $(\text{LTO})_1/(\text{STO})_1$ superlattice, the DOS for both *d*_{xy} and *d*_{yz} (*d*_{xz}) orbitals gradually increases with energy as shown in Fig. 3(a). In the

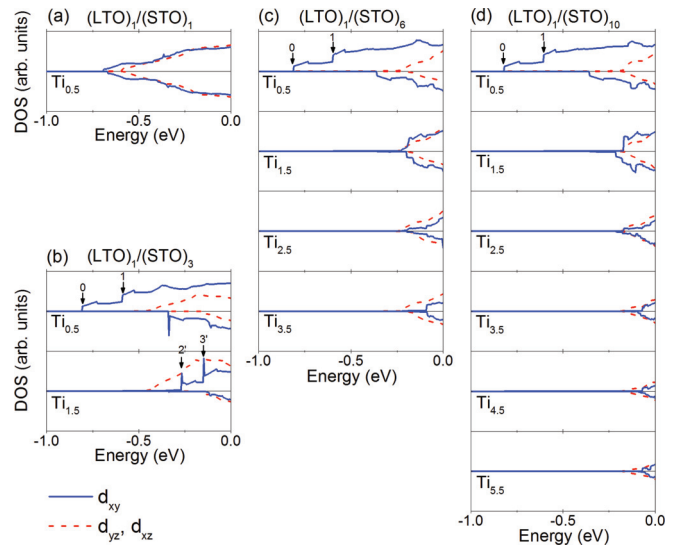


FIG. 3. (Color online) Ti 3*d* DOS for conduction bands at Ti atoms for (a) $(\text{LTO})_1/(\text{STO})_1$, (b) $(\text{LTO})_1/(\text{STO})_3$, (c) $(\text{LTO})_1/(\text{STO})_6$, and (d) $(\text{LTO})_1/(\text{STO})_{10}$ superlattices. The Fermi level is at 0 eV. At each Ti site, the DOS with spin-up (spin-down) states is shown in the upper (lower) panel. The *d*_{xy} orbital is blue (solid line), while the degenerate *d*_{yz} and *d*_{xz} states are red (dashed line).

(LTO)₁/(STO)₃ superlattice, the shape of d_{xy} DOS becomes different from the d_{yz} (d_{xz}) DOS. As shown in Fig. 3(b), the DOS of d_{xy} spin-up states at the Ti_{0.5} site exhibits the staircaselike increments at -0.82 eV and -0.60 eV (marked as 0 and 1). Interestingly, these staircaselike increments remain the same for thicker STO spacers, as shown in Figs. 3(c) and 3(d). Such a staircase increment in DOS is a well-known feature of 2DEGs with quantized energy levels due to wave function confinements. In the (LTO)₁/(STO)_N superlattices with $N \geq 3$ u.c., the d_{xy} orbital electrons at Ti_{0.5} sites are 2DEGs confined in the LaO-induced potential wells with the discrete energy levels of -0.82 eV and -0.60 eV.

In the (LTO)₁/(STO)₃ structure, the d_{xy} DOS has other staircase increments at the Ti_{1.5} site but at higher energy levels of -0.287 eV and -0.162 eV [marked as 2' and 3' in Fig. 3(b)]. This can be explained by the distributions of 2DEGs in a wedge/triangular potential well; electrons at low energy are localized near the potential valley, but electrons at high energy stay away from the potential valley.^{10,37} The presence of d_{xy} 2DEGs at discrete energy levels also explains the multichannel conduction from experiments.⁵ The DOS of d_{yz} (d_{xz}) orbital does not show staircaselike increments. Generally, it increases with energy indicating that the d_{yz} (d_{xz}) orbital has 3D transport characteristics.

To confirm the transport dimensionality of d orbitals, the transport directivity has been investigated by calculating electron effective masses from band structures. Figure 4 shows the calculated band structures for spin-up states within the first Brillouin zone. The Fermi level is at 0 eV. In the (LTO)₁/(STO)₁ structure, the d_{xy} band is the lowest conduction band at -0.714 eV at the Γ point, and the d_{yz} (d_{xz}) band is the second lowest conduction band at -0.605 eV. Using the parabolic approximation near the Γ point, the electron effective masses

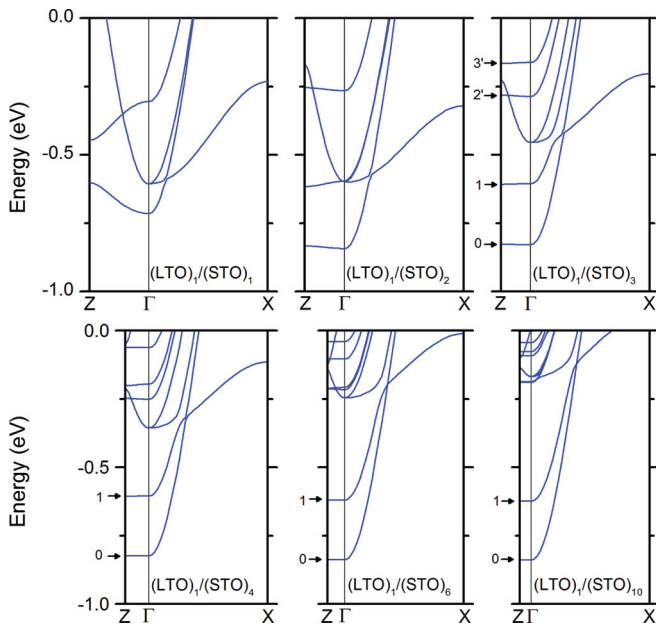


FIG. 4. (Color online) Band structures of (LTO)₁/(STO)_N superlattices for spin-up states within the first Brillouin zone. Only conduction bands are shown here. The Fermi level is at 0 eV. The bands 0, 1, 2', and 3' correspond to the increments in d_{xy} DOS in Fig. 3.

of the lowest d_{xy} band are calculated as $m_{xx} = 0.40 m_0$ and $m_{zz} = 2.67 m_0$, parallel and perpendicular to the interfaces, respectively. In the (LTO)₁/(STO)₂ structure, the lowest d_{xy} band moves down to -0.83 eV, which is lower than the d_{yz} (d_{xz}) band by 0.246 eV at the Γ point. In the (LTO)₁/(STO)₂ structure, the electron effective mass of the lowest d_{xy} band has increased to $m_{zz} = 10.8 m_0$ perpendicular to the interfaces, but it remains the same as $m_{xx} = 0.40 m_0$ along the interfaces. In the (LTO)₁/(STO)₃ structure, the lowest d_{xy} band (marked as 0) becomes almost flat along the Γ -Z direction, which implies that the kinetic energy is independent from k_z . Since the effective mass is inversely proportional to the band curvature at the Γ point, the electrons in the lowest d_{xy} band in the (LTO)₁/(STO)₃ structure are extremely heavy to transport perpendicularly to the interfaces, but they can still transport along the interfaces with the effective mass of $m_{xx} = 0.40 m_0$. Furthermore, the lowest d_{xy} band in the (LTO)₁/(STO)₃ band structure is at -0.83 eV, which is very close to the first staircase increment in the d_{xy} spin-up DOS at the Ti_{0.5} site [see Fig. 3(b)]. Therefore, the lowest d_{xy} band in the (LTO)₁/(STO)₃ superlattice is the 2DEG, which can travel only along the interface due to the confinement by the LaO-induced potential well.

The second lowest d_{xy} band is also the 2DEG at -0.61 eV (marked as 1), corresponding to the second staircase increment in the d_{xy} DOS at the Ti_{0.5} site [see Fig. 3(b)]. These two lowest d_{xy} bands (0 and 1) also remain the same for $N \geq 3$ u.c., as shown in Fig. 4. Unlike d_{xy} bands, the d_{yz} (d_{xz}) bands have constant electron effective masses as $m_{xx} = 0.50 m_0$ and $m_{zz} = 0.45 m_0$ for all STO thicknesses, which confirms that the d_{yz} (d_{xz}) orbital electrons have 3D transport property in (LTO)₁/(STO)_N superlattices.

Electron densities of d orbitals are shown in Fig. 5 as a function of STO thickness. In the (LTO)₁/(STO)₁ superlattice, the d_{xy} electron density is slightly higher than the d_{yz} (d_{xz}) electrons. As the STO thickness increases, the d_{xy} electron density increases, while the d_{yz} (d_{xz}) electron density decreases. Since the 2DEG is formed by d_{xy} orbital electrons when $N \geq 3$ u.c. only and the d_{yz} (d_{xz}) orbital electrons always

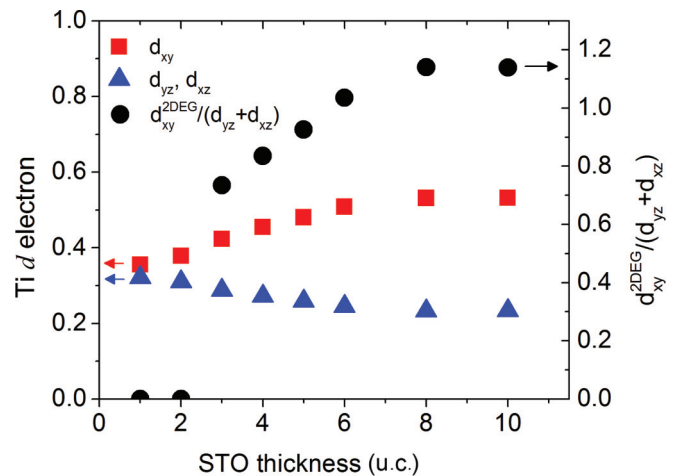


FIG. 5. (Color online) Normalized electron densities of d_{xy} and d_{yz} (d_{xz}) orbitals as a function of STO thickness and the ratio of 2DEG to 3D electrons as $d_{xy}^{2DEG}/(d_{yz} + d_{xz})$ with $d_{xy}^{2DEG} = 0$ for $N < 3$ u.c.

have 3D transport characteristic, the transport dimensionality of $(\text{LTO})_1/(\text{STO})_N$ superlattices starts to change from 3D to 2D at $N = 3$ u.c. The ratio of 2D to 3D electrons can be estimated as $d_{xy}^{2\text{DEG}}/(d_{yz} + d_{xz})$ with taking $d_{xy}^{2\text{DEG}} = 0$ for $N < 3$ u.c., as shown in Fig. 5. The convergence of d_{xy} and $(d_{yz} + d_{xz})$ electron densities at $N = 8$ u.c. is due to the large separation distance between the neighboring potentials.

IV. CONCLUSION

The effects of STO spacer thickness on the transport dimensionality of d orbital electrons in $(\text{LTO})_1/(\text{STO})_N$ superlattices have been investigated using DFT calculations with the LSDA + U method. The d_{xy} orbital electrons are highly localized near interfaces due to the potentials by the positively charged LaO layers, while the degenerate d_{yz} and

d_{xz} orbital electrons are more distributed inside the STO insulators. As the STO thickness increases, the occupancy of d_{yz} (d_{xz}) orbital decreases drastically and becomes almost uniform. For $N \geq 3$ u.c., the Ti d_{xy} DOS shows the staircaselike increments, which appear at the same energy levels of d_{xy} flat bands along Γ -Z direction in band structures. These k_z -independent discrete energy levels indicate that the electrons in d_{xy} flat bands are 2DEGs that can transport along interfaces but cannot transport perpendicularly to interfaces due to the confinements in the potential wells by LaO layers. Unlike d_{xy} orbital electrons, the d_{yz} and d_{xz} orbital electrons always have 3D transport characteristics. The formation of the d_{xy} 2DEG for $N \geq 3$ u.c. indicates that the electron transport dimensionality in $(\text{LaTiO}_3)_1/(\text{SrTiO}_3)_N$ superlattices starts to change from 3D to 2D with the STO thickness of 3 u.c.

*Corresponding author: jyou@smu.edu

¹A. Ohtomo, D. A. Muller, J. L. Grazul, and H. Y. Hwang, *Nature* **419**, 378 (2002).

²A. Ohtomo and H. Y. Hwang, *Nature* **427**, 423 (2004).

³N. Nakagawa, H. Y. Hwang, and D. A. Muller, *Nat. Mater.* **5**, 204 (2006).

⁴J. Mannhart and D. G. Schlom, *Science* **327**, 1607 (2010).

⁵J. S. Kim, S. S. A. Seo, M. F. Chisholm, R. K. Kremer, H. U. Habermeier, B. Keimer, and H. N. Lee, *Phys. Rev. B* **82**, 201407(R) (2010).

⁶A. D. Caviglia, S. Gariglio, C. Cancellieri, B. Sacepe, A. Fete, N. Reyren, M. Gabay, A. F. Morpurgo, and J. M. Triscone, *Phys. Rev. Lett.* **105**, 236802 (2010).

⁷S. L. Chuang, *Physics of Optoelectronic Devices* (John Wiley & Sons, Inc., New York, 1995).

⁸J. H. Davies, *The Physics of Low-dimensional Semiconductors: An Introduction* (Cambridge University Press, New York, 1997).

⁹S. Su, J. H. You, and C. Lee, *J. Appl. Phys.* **113**, 093709 (2013).

¹⁰J. Biscaras, N. Bergeal, S. Hurand, C. Grossetete, A. Rastogi, R. C. Budhani, D. LeBoeuf, C. Proust, and J. Lesueur, *Phys. Rev. Lett.* **108**, 247004 (2012).

¹¹W. S. Choi, S. Lee, V. R. Cooper, and H. N. Lee, *Nano Lett.* **12**, 4590 (2012).

¹²H. Ohta, S. Kim, Y. Mune, T. Mizoguchi, K. Nomura, S. Ohta, T. Nomura, Y. Nakanishi, Y. Ikuhara, M. Hirano, H. Hosono, and K. Koumoto, *Nat. Mater.* **6**, 129 (2007).

¹³Y. Mune, H. Ohta, K. Koumoto, T. Mizoguchi, and Y. Ikuhara, *Appl. Phys. Lett.* **91**, 192105 (2007).

¹⁴H. Ohta, Y. Mune, K. Koumoto, T. Mizoguchi, and Y. Ikuhara, *Thin Solid Films* **516**, 5916 (2008).

¹⁵Y. Kozuka, M. Kim, C. Bell, B. G. Kim, Y. Hikita, and H. Y. Hwang, *Nature* **462**, 487 (2009).

¹⁶M. Basletic, J. L. Maurice, C. Carretero, G. Herranz, O. Copie, M. Bibes, E. Jacquet, K. Bouzehouane, S. Fusil, and A. Barthelémy, *Nat. Mater.* **7**, 621 (2008).

¹⁷R. Ohtsuka, M. Matvejeff, K. Nishio, R. Takahashi, and M. Lippmaa, *Appl. Phys. Lett.* **96**, 192111 (2010).

¹⁸N. Reyren, S. Thiel, A. D. Caviglia, L. F. Kourkoutis, G. Hammerl, C. Richter, C. W. Schneider, T. Kopp, A. S. Ruetschi, D. Jaccard, M. Gabay, D. A. Muller, J. M. Triscone, and J. Mannhart, *Science* **317**, 1196 (2007).

¹⁹J. Biscaras, N. Bergeal, A. Kushwaha, T. Wolf, A. Rastogi, R. C. Budhani, and J. Lesueur, *Nature Commun.* **1**, 89 (2010).

²⁰A. D. Caviglia, S. Gariglio, N. Reyren, D. Jaccard, T. Schneider, M. Gabay, S. Thiel, G. Hammerl, J. Mannhart, and J. M. Triscone, *Nature* **456**, 624 (2008).

²¹A. Brinkman, M. Huijben, M. Van Zalk, J. Huijben, U. Zeitler, J. C. Maan, W. G. Van der Wiel, G. Rijnders, D. H. A. Blank, and H. Hilgenkamp, *Nat. Mater.* **6**, 493 (2007).

²²L. Li, C. Richter, J. Mannhart, and R. C. Ashoori, *Nat. Phys.* **7**, 762 (2011).

²³J. A. Bert, B. Kalisky, C. Bell, M. Kim, Y. Hikita, H. Y. Hwang, and K. A. Moler, *Nat. Phys.* **7**, 767 (2011).

²⁴B. Jalan and S. Stemmer, *Appl. Phys. Lett.* **97**, 042106 (2010).

²⁵S. Thiel, G. Hammerl, A. Schmehl, C. W. Schneider, and J. Mannhart, *Science* **313**, 1942 (2006).

²⁶H. Ishida and A. Liebsch, *Phys. Rev. B* **77**, 115350 (2008).

²⁷V. R. Cooper, *Phys. Rev. B* **85**, 235109 (2012).

²⁸P. Larson, Z. S. Popović, and S. Satpathy, *Phys. Rev. B* **77**, 245122 (2008).

²⁹D. R. Hamann, D. A. Muller, and H. Y. Hwang, *Phys. Rev. B* **73**, 195403 (2006).

³⁰S. Okamoto, A. J. Millis, and N. A. Spaldin, *Phys. Rev. Lett.* **97**, 056802 (2006).

³¹P. V. Ong, J. Lee, and W. E. Pickett, *Phys. Rev. B* **83**, 193106 (2011).

³²G. Kresse and J. Furthmüller, *Phys. Rev. B* **54**, 11169 (1996).

³³G. Kresse and D. Joubert, *Phys. Rev. B* **59**, 1758 (1999).

³⁴P. E. Blöchl, *Phys. Rev. B* **50**, 17953 (1994).

³⁵A. I. Liechtenstein, V. I. Anisimov, and J. Zaanen, *Phys. Rev. B* **52**, R5467 (1995).

³⁶T. Mizokawa and A. Fujimori, *Phys. Rev. B* **51**, 12880 (1995).

³⁷Z. S. Popovic and S. Satpathy, *Phys. Rev. Lett.* **94**, 176805 (2005).